Contrast-enhanced microCT evaluation of degeneration following partial and full width injuries to mouse lumbar intervertebral disc

+Remy E. Walk, MS[1,2]; +Hong Joo Moon, MD, PhD[2,3]; Simon Y. Tang, PhD, MSCI [1,2]

Munish C. Gupta, MD[2]

[1] Dept of Biomedical Engineering, Washington University in St. Louis, St. Louis, MO, USA
[2] Dept of Orthopaedic Surgery, Washington University in St. Louis, St. Louis, MO, USA
[3] Dept of Neurosurgery, Korea University College of Medicine, Seoul, South Korea

+ These authors contributed equally.

Keywords: Lumbosacral surgical exposure; Intervertebral disc degeneration; annulus fibrosus injury; mouse model

Abstract

Study Design: Preclinical animal study

Objective: Evaluation of the degenerative progression resulting from either a partial- or full- width injury to the mouse lumbar intervertebral disc (IVD) using contrast-enhanced micro-computed tomography and histological analyses. We utilized a lateral-retroperitoneal surgical approach to access the lumbar IVD, and the injuries to the IVD were induced by either incising one side of the annulus fibrosus or puncturing both sides of the annulus fibrosus. The full-width injury caused dramatic reduction in nucleus pulposus hydration and significant degeneration. A partial-width injury produces localized deterioration around the annulus fibrosus site that resulted in local tissue remodeling without gross degeneration to the IVD.

Methods: Female C57BL/6J mice of 3-4 months age were used in this study. They were divided into three groups to undergo a partial-width, full-width, or sham injuries. The L5/L6 and L6/S1 lumbar IVDs were surgically exposed using a lateral-retroperitoneal approach. The L6/S1 IVDs were injured using either a surgical scalpel (partial-width) or a 33G needle (full-width), with the L5/L6 serving as an internal control. These animals were allowed to recover and then sacrificed at 2-, 4-, or 8- weeks post-surgery. The IVDs were assessed for degeneration using contrast-enhanced microCT (CEμCT) and histological analysis.

Results: The high-resolution 3D evaluation of the IVD confirmed that the respective injuries localized within one side of the annulus fibrosus or spanned the full width of the IVD. The full-width injury caused deteriorations in the nucleus pulposus after 2 weeks that culminated in significant degeneration at 8 weeks, while the partial width injury caused localized disruptions that remained limited to the annulus fibrosus.

Conclusion: The use of CEμCT revealed distinct IVD degeneration profiles resulting from partial- and full- width injuries. The partial width injury may serve as a better model for IVD degeneration resulting from localized annulus fibrosus injuries in humans.

Introduction

Mouse models are often used for the preclinical validation of treatments and therapeutic candidates. Mice offer particular advantages of relatively easy maintenance, year-round breeding with a short gestation period, delivery of large litters, and inbred tolerance[1]. Furthermore, the ability to manipulate the mouse genome enables mechanistic studies with greater biological precision than larger mammalian models including rats, rabbits, and pigs[1]. Moreover, the mouse lumbar intervertebral disc (IVD) provides close geometric and microstructural semblance to the human lumbar IVD compared to other preclinical animal models[2]. While the mouse lumbar IVD exhibits age-related degeneration[3,4], an injury is often utilized to reproduce the inflammatory conditions and accelerate the IVD's degenerative cascade[5,6].

To create a targeted injury to the IVD, surgical exposure of the IVD is required. These commonly involve the posterior-lateral, transperitoneal, and anterior/lateral retroperitoneal surgical access. Of these, the retroperitoneal approach offers multiple advantages: (1) minimal damage to major organs, vessels, and musculature; (2) access to multiple levels with a relatively small incision; and (3) visual availability of the target tissue under microscopy. Moss et al. demonstrated the efficacy and reproducibility of the retroperitoneal approach in rabbits [7]. Exposing the lumbar IVD enables the ability to create a targeted, directed injury for the investigation of the subsequent degenerative process [8–10]. Masuda et al. and Sobajima et al. described the rabbit annulus fibrosus injury model where the injury was confined to the annulus fibrosus that caused slow progressive degeneration of the IVD over 8 weeks. The phenotype and the progressive nature of this model recapitulates the human disease, and may be better suited to explore therapies that leverage biological regenerative strategies. In contrast, more damaging approaches that injures both the annulus fibrosus and nucleus pulposus produce rapid and severe course of degeneration [7,11]. There are several studies describing IVD degeneration using the lumbosacral IVD injury in the mouse model[12–14]. In the mouse IVD where the average disc height is approximately 300-400 microns, an injury by needle puncture produces damage to 55-90% across the height and 15-40% across the width of the IVD[2,11], representing significant trauma that is atypical in human IVDs. Moreover, these procedures

involve damage and injury to the nucleus pulposus, such as with a complete puncture to the IVD, with no possibility to decouple the contributions of the annulus fibrosus and the nucleus pulposus toward the ensuing degenerative cascade. Piazza and coauthors have shown that unilateral (half-width) and bilateral (full-width) injuries in the tail IVD results in unique degenerative trajectories, but this has not been investigated in the mouse lumbar spine. We thus sought to compare the degenerative profiles of IVDs after partial- and full- width injuries in the mouse lumbar spine. In order to evaluate the degeneration of the IVD in a spatially robust manner, we utilized contrast-enhanced microCT[15,16], in addition to histological grading, to quantify the changes in structure and composition at 2-, 4- and 8- weeks after surgery.

Materials and Methods

Animal Preparation

All procedures were performed following Washington University School of Medicine IACUC approval. Female C57BL/6J mice of 3-4 months age were used (BW: 20 – 25 g). They were housed under standard animal husbandry conditions (in a temperature-controlled [21 ± 1°C] room with normal 12-hr light/dark cycles). These animals were divided into three groups: Partial-width injury (PW), full-width injury (FW), and Sham (n=15-18 per group) with all animals undergoing to retroperitoneal surgical exposure of the lumbar IVD. The groups were cross-sectionally evaluated at 2-, 4-, and 8- week post-surgery time points. The injury was delivered to the L6/S1 IVD with the L5/6 IVD used as the internal control.

The partial-width injury mimics a localized injury to the annulus fibrosus, aka annular tear injury, in humans[17]. To evaluate the feasibility of this injury, we first performed the partial-width injury on six animals, and then they were euthanized shortly after recovery from anesthesia. The IVDs were harvested and measured for the thickness of the annulus fibrosus and the depth of the injury using contrast-enhanced microCT (CEμCT) and histological analysis.

The second set of animals were allowed to recover following PW, FW or Sham surgery for 2, 4 or 8 weeks (n = 5-6 per group) and then euthanized, and the IVD tissues were assessed for degeneration with CEμCT and histological analysis. Samples where attenuation was saturated were not included in analysis.

Mice were anesthetized with isoflurane gas in oxygen via a facemask (3–4% induction and 2–2.5% maintenance at 1 L/min flow rate; Highland Medical Equipment) and were given a preoperative intradermal injection of lidocaine (7 mg/kg; Hospira, Inc). The left flank was then shaved from the ventral to the dorsal midlines, and the skin was sterilized. The skin was prepared for aseptic surgery via washing with 70% ethanol and povidone iodine.

Partial-width injury: A distance of 0.3 mm from the end of the No. 11-scalpel blade tip was measured and marked with a micro-caliper under a microscope (Figure 1). The distance of 0.3 mm was determined from our preliminary studies. The edge of the blade was allowed to insert into the IVD until the 0.3 mm marking was no long visible under the microscope. Once pierced, the injury site was closely observed under the microscope to confirm that there is no leakage of the NP.

Full-width injury: A 33G needle was inserted bilaterally through the IVD lateral axis of the IVD. In contrast to the partial-width injury, NP herniations were observed following the full-width injury.

Contrast-enhanced microCT tomography (CEμCT): Samples were incubated in a solution of 175 mg/mL solution diluted from a stock of OptiRay 350 (Guerbet, St. Louis) in PBS at 37°C. After 24 hrs of incubation, samples were scanned using a μCT40 (Scanco Medical, CH) at a 10-μm voxel size (45 kVp, 177 uA, high resolution, 300 ms integration).

CEμCT data was exported as a DICOM file for analysis in a custom MATLAB program. After an initial median filter (sigma = 0.8, support = 5), functional spine units were isolated from surrounding soft tissue not part of the IVD by drawing a contour around the outer edge every 5 transverse slices and morphing using linear interpolation. The IVD was manually segmented from the vertebral bodies with the same methodology as above. The remaining voxels were designated as the whole disc mask. The NP was thresholded from the AF followed by a morphological close and morphological open to fill interior holes and smooth the boundary. The volumes and average attenuations (intensity) were calculated from the mask of the NP and whole disc. The volume was determined from the total number of voxels contained within the mask and the attenuation was taken as the average 16-bit grayscale value of the voxels. Visualizations of the microCT were obtained using the image processing application OsiriX (Pixmeo, Geneva). AF thickness, partial-width injury depth and disc height index (DHI) were measured along the mid-sagittal plane. DHI was calculated as the ratio of the IVD height to width. IVD height was taken as the average at 5 equidistant points along the mid-sagittal plane. The ratio of NP intensity/disc intensity (NI/DI), defined as the average attenuation of voxels in the NP mask divided by the full disc mask, is an unbiased, fully

three-dimensional measure that quantifies the relative size and hydration to inform the relative changes in degeneration [18].

Histological analysis: Following microCT, samples were fixed for 24 hours in 10% neutral buffered formalin followed by 3 days of decalcification in Immunocal (StatLab 1414-X). The samples were embedded in paraffin, sectioned at a thickness of 10 μm, and then stained with Safranin-O and Fast Green.

Measuring thickness of AF and the depth of partial-width injury: The CEμCT of the injured L6/S1 and histological analysis on uninjured L5/6 were used to measure the thickness of the AF. The CEμCT on the injured L6/S1 was used to measure the depth of injury as defined by the shortest perpendicular distance from the outer edge of annulus fibrosus to the visually observable outline of the injury site.

Assessment of IVD degeneration: Histological classification system recently developed by Melgoza et al. in 2021 was used to quantify the degeneration of the injured level (L6/S1) which allows the independent evaluation of the nucleus pulposus, annulus fibrosus, endplates and interface boundaries[19]. Morphology and NI/DI determined from CEμCT was used to further inform the level of degeneration of the injured level (L6/S1) compared to the internal control (L5/6).

Results

A total of 57 mice were subjected to the surgical procedure. The average surgery time was 15 min 38 sec ± 6 min 23 sec from incision to closure. There was no mortality or severe complication such as massive bleeding due to vascular injury during surgery. Caution was taken to prevent injury of the lumbosacral plexus located posteriorly during the blunt dissection of the psoas muscle from posterior to the anterior direction.

Annulus Fibrosus (AF) Thickness

CEμCT and histology measurements of AF thickness and IVD width were highly consistent. The anteroposterior IVD width measured with CEμCT was 1.27 ± 0.13 mm (mean ± standard deviation), whereas that measured by histological analysis was 1.21 ± 0.11 mm. AF thickness measured with CEμCT was 0.38±0.05 mm and that measured with histological analysis was 0.43 ± 0.10 mm (Figure 3). The CEμCT measured values were statistically indistinguishable from ($p = 0.37$) and were highly correlated ($r^2 = 0.96$) with the histologically measured values (Figure 2).

Depth of Partial-width Injury

All injuries except one were isolated to the AF (Figure 3B). In sample 5, the NP may have been injured because CEμCT showed disruption of the AF/NP boundary (Figure 3C). The depth of injury measured with CEμCT was 0.29 ± 0.05 mm. The ratio of the injury depth to the AF thickness was 0.80 ± 0.19 (Figure 3D and 3E).

Structural evaluation of the IVD

Neither the partial-width nor the full-width injuries resulted in changes in the Disc Height Index across the two-, four-, and eight- week time points (Figure 4D). Similarly, the size of the nucleus pulposus, characterized by the nucleus pulposus (NP) volume fraction, were not dramatically different between groups and time points (Figure 4E). The relative hydration of the NP, quantified by the ratio of NP attenuating intensity to that of the whole disc (NI/DI), revealed the full-width injury caused a dramatic

decrease in the attenuation of the NP at the two- and four- week time points, with a trending change at eight- weeks. Reduced NI/DI indicates a loss of NP hydration.

The impact of the partial- and full- width injuries to the annulus fibrosus was observable at two weeks, The relative hydration of the annulus fibrosus (AF) increases after an injury, and this is evident in both the partial- and full- width groups. Two weeks after injury, both the partial- and full- injuries showed an increase attenuation of the AF, with the full-width injury group sustaining this increase (Figure 4G).

Extent of IVD Degeneration

Quantitative histological analyses revealed a differential degenerative cascade to the IVD following full-width injury as early as two weeks post injury but not with the partial-width injury. The histological classification showed significant degeneration following FW injury at all timepoints ($p < 0.05$) in the NP, AF, interface boundaries, and total IVD score but not endplate score compared to Sham while no differences were detected between PW and Sham (Figure 5). No morphological differences between timepoints or injury groups were observed.

Discussion

Animal models of IVD degeneration are imperative to elucidate the key molecular mechanisms of the pathophysiology. To date, rodents, rabbits, dogs, goats, sheep, and primates have been used as models for intervertebral disc degeneration[20]. One main advantage of mouse models is the availability of reagents and modifications that could be used concomitantly with surgically induced IVD degeneration. However, the small size of the mouse requires a high degree of surgical precision, particularly with access and exposure of the lumbar spine. While many studies utilize the mouse tail for degenerative models[12,21–23], the lumbar spine maintains the anatomical proximity to physiologically relevant structures such as the dorsal root ganglions and may better recapitulate the human disease[22].

We describe here a novel procedure for mouse lumbosacral IVD injury with visual guidance via microscopy and gross features. The retroperitoneal space of the spine can be located (Figure S1) with the left pelvic bone with gluteus muscles and proximal thigh as landmarks (Figure 1C and 1D). Blunt-dissection of the fat pad surrounding the thoracic cage anteriorly, the gluteus muscles superiorly, and the thigh muscles posteriorly (Figure 1B) exposes these two landmarks (Figure 1C). The lateral approach to the IVD allows for precise injury to the annulus fibrosus of the IVD (Figure 1). Exposure of the pelvic bone from the gluteus muscle and rotation of the pelvic bone posteriorly is necessary to achieve ample exposure of multiple IVDs in the surgical field. The psoas muscles can be easily scraped posterior-anteriorly with a Penfield dissector. CEμCT allowed for a 3D spatially unbiased quantification of morphology and composition[18] that confirmed the localization of injury across the cross-section time points. CEμCT measurements of the IVD morphology were in excellent agreement with histological measures. NI/DI and histological analysis indicated degeneration of injured IVDs starting 4 weeks post-surgery.

The present study describes a surgical procedure to expose the lumbosacral spine of mice and to induce a localized experimental injury with AF-limited depth and compared the degenerative response with a more commonly used needle puncture injury. The technique described herein also focused on achieving a consistent depth and size of injury. The marked tip of the No. 11-scalpel blade tip was confirmed with

CEμCT to provide AF-limited injury and resulted in no NP leakage under observation by microscopy. The various sizes of the needle may produce inconsistent depth and size of injury. A thick needle may lead to end-plate injury due to the small IVD height in mice, whereas the excessive flexibility of a thin needle would contribute to inconsistency in the depth of injury. While most injury models cause damage to the nucleus pulposus, the cartilaginous endplates , and even the vertebral body[24–26], the partial-width injury here results in an isolated injury to the outer annulus fibrosus. Surprisingly, we observed no degenerative changes in the endplate in the full-width injury, suggesting that it is possible to induce an IVD only injury using a carefully applied 33G needle. Following full-width injury, IVDs exhibited quick and sustained degeneration as early as two weeks after injury, and this is sustained through the four- and eight- week time points. Despite maintaining disc height, the FW injury caused consistent degenerative changes in the nucleus pulposus, annulus fibrosus, and interface boundaries which included the AF-endplate and NP-AF boundaries. The PW injury did not produce statistically significant degenerative changes, but whether the innervation or vascularization profile changes particularly at the outer annulus fibrosus remains to be investigated.

CEμCT allowed for visualization of the injury site following both partial- and full- width injuries. The increased attenuation on CEμCT may indicate changes in composition or diffusion properties resulting from the disruption in the annulus fibrosus with both injuries. The injured annulus fibrosus appears to be highly hydrated, due to the increased interstitial fluids that localize around the injury site (Figures 3 -4). Since IVD degeneration in humans often starts as a tear in the annulus fibrosus [17], this model will enable mechanistic investigations of how injuries of the annulus fibrosus contribute to IVD degeneration and the subsequent development of low back pain. In contrast, the full-width injury to the nucleus pulposus induces a more rapid and severe course of degeneration that is more aligned with an acute trauma [7,20,21]. Unlike the increased attenuation of the injured annulus fibrosus, the depressurized nucleus pulposus loses water and attenuates less than the healthy state (Figures 4). Consistent with unilateral injuries of the tail IVD, the resultant degenerative cascade was nuanced[11], and required high resolutions modalities to detect measurable

changes. Future studies will evaluate the partial-width injury as a slowly progressing IVD degeneration model following a clinically relevant injury.

References

1. Rao RD, Bagaria VB, Cooley BC. Posterolateral intertransverse lumbar fusion in a mouse model: surgical anatomy and operative technique. *Spine J*. 2007;7(1):61-67. doi:10.1016/J.SPINEE.2006.03.004

2. O'Connell GD, Vresilovic EJ, Elliott DM. Comparison of animals used in disc research to human lumbar disc geometry. *Spine (Phila Pa 1976)*. 2007;32(3):328-333. doi:10.1097/01.BRS.0000253961.40910.C1

3. Gruber HE, Sage EH, Norton HJ, Funk S, Ingram J, Hanley EN. Targeted deletion of the SPARC gene accelerates disc degeneration in the aging mouse. *J Histochem Cytochem*. 2005;53(9):1131-1138. doi:10.1369/JHC.5A6687.2005

4. Dahia CL, Mahoney EJ, Durrani AA, Wylie C. Postnatal growth, differentiation, and aging of the mouse intervertebral disc. *Spine (Phila Pa 1976)*. 2009;34(5):447-455. doi:10.1097/BRS.0B013E3181990C64

5. Lotz JC, Hsieh AH, Walsh AL, Palmer EI, Chin JR. Mechanobiology of the intervertebral disc. *Biochem Soc Trans*. 2002;30(Pt 6):853-858. doi:10.1042/BST0300853

6. Abraham AC, Liu JW, Tang SY. Longitudinal Changes in the Structure and Inflammatory Response of the Intervertebral Disc Due to Stab Injury in a Murine Organ Culture Model. *J Orthop Res*. 2016;34(8):1431. doi:10.1002/JOR.23325

7. Moss IL, Zhang Y, Shi P, Chee A, Piel MJ, An HS. Retroperitoneal approach to the intervertebral disc for the annular puncture model of intervertebral disc degeneration in the rabbit. *Spine J*. 2013;13(3):229-234. doi:10.1016/J.SPINEE.2012.02.028

8. Lotz JC. Animal models of intervertebral disc degeneration: lessons learned. *Spine (Phila Pa 1976)*. 2004;29(23):2742-2750. doi:10.1097/01.BRS.0000146498.04628.F9

9. Masuda K, Lotz JC. New challenges for intervertebral disc treatment using regenerative medicine. *Tissue Eng Part B Rev*. 2010;16(1):147-158. doi:10.1089/TEN.TEB.2009.0451

10. Vo N, Niedernhofer LJ, Nasto LA, et al. An overview of underlying causes and animal models for the study of age-related degenerative disorders of the spine and synovial joints. *J Orthop Res*. 2013;31(6):831-837. doi:10.1002/JOR.22204

11. Piazza M, Peck SH, Gullbrand SE, et al. Quantitative MRI correlates with histological grade in a percutaneous needle injury mouse model of disc degeneration. *J Orthop Res*. 2018;36(10):2771-2779. doi:10.1002/JOR.24028

12. Shi C, Das V, Li X, et al. Development of an in vivo mouse model of discogenic low back pain. *J Cell Physiol*. 2018;233(10):6589-6602. doi:10.1002/jcp.26280

13. Ohnishi T, Sudo H, Iwasaki K, Tsujimoto T, Ito YM, Iwasaki N. In Vivo Mouse Intervertebral Disc Degeneration Model Based on a New Histological Classification. *PLoS One*. 2016;11(8):e0160486. doi:10.1371/JOURNAL.PONE.0160486

14. Millecamps M, Stone LS. Delayed onset of persistent discogenic axial and radiating pain after a single-level lumbar intervertebral disc injury in mice. *Pain*. 2018;159(9):1. doi:10.1097/j.pain.0000000000001284

15. Lin KH, Wu Q, Leib DJ, Tang SY. A novel technique for the contrast-enhanced microCT imaging of murine intervertebral discs. *J Mech Behav Biomed Mater*. 2016;63:66-74. doi:10.1016/j.jmbbm.2016.06.003

16. Walk RE, Tang SY. In vivo contrast-enhanced microCT for the monitoring of mouse thoracic,

lumbar, and coccygeal intervertebral discs. *JOR spine*. 2019;2(2). doi:10.1002/JSP2.1058

17. Berger-Roscher N, Galbusera F, Rasche V, Wilke HJ. Intervertebral disc lesions: visualisation with ultra-high field MRI at 11.7 T. *Eur Spine J*. 2015;24(11):2488-2495. doi:10.1007/S00586-015-4146-0

18. Lin KH, Tang SY. The Quantitative Structural and Compositional Analyses of Degenerating Intervertebral Discs Using Magnetic Resonance Imaging and Contrast-Enhanced Micro-Computed Tomography. *Ann Biomed Eng*. 2017;45(11):2626-2634. doi:10.1007/S10439-017-1891-8/FIGURES/6

19. Melgoza IP, Chenna SS, Tessier S, et al. Development of a standardized histopathology scoring system using machine learning algorithms for intervertebral disc degeneration in the mouse model—An ORS spine section initiative. *JOR Spine*. 2021;4(2):e1164. doi:10.1002/JSP2.1164

20. Masuda K, Aota Y, Muehleman C, et al. A novel rabbit model of mild, reproducible disc degeneration by an anulus needle puncture: Correlation between the degree of disc injury and radiological and histological appearances of disc degeneration. *Spine (Phila Pa 1976)*. 2005;30(1):5-14. doi:10.1097/01.BRS.0000148152.04401.20

21. Sobajima S, Kompel JF, Kim JS, et al. A slowly progressive and reproducible animal model of intervertebral disc degeneration characterized by MRI, X-ray, and histology. *Spine (Phila Pa 1976)*. 2005;30(1):15-24. doi:10.1097/01.BRS.0000148048.15348.9B

22. Tian Z, Ma X, Yasen M, et al. Intervertebral Disc Degeneration in a Percutaneous Mouse Tail Injury Model. *Am J Phys Med Rehabil*. 2018;97(3):170-177. doi:10.1097/PHM.0000000000000818

23. Yang F, Leung VYL, Luk KDK, Chan D, Cheung KMC. Injury-induced sequential transformation of notochordal nucleus pulposus to chondrogenic and fibrocartilaginous phenotype in the mouse. *J Pathol*. 2009;218(1):113-121. doi:10.1002/PATH.2519

24. Jin L, Balian G, Li XJ. Animal Models for Disc Degeneration-an Update. *Histol Histopathol*. 2018;33(6):543. doi:10.14670/HH-11-910

25. Cunha C, Lamas S, Gonçalves RM, Barbosa MA. Joint analysis of IVD herniation and degeneration by rat caudal needle puncture model. *J Orthop Res*. 2017;35(2):258-268. doi:10.1002/JOR.23114

26. Elliott DM, Yerramalli CS, Beckstein JC, Boxberger JI, Johannessen W, Vresilovic EJ. The effect of relative needle diameter in puncture and sham injection animal models of degeneration. *Spine (Phila Pa 1976)*. 2008;33(6):588-596. doi:10.1097/BRS.0B013E318166E0A2

Figures

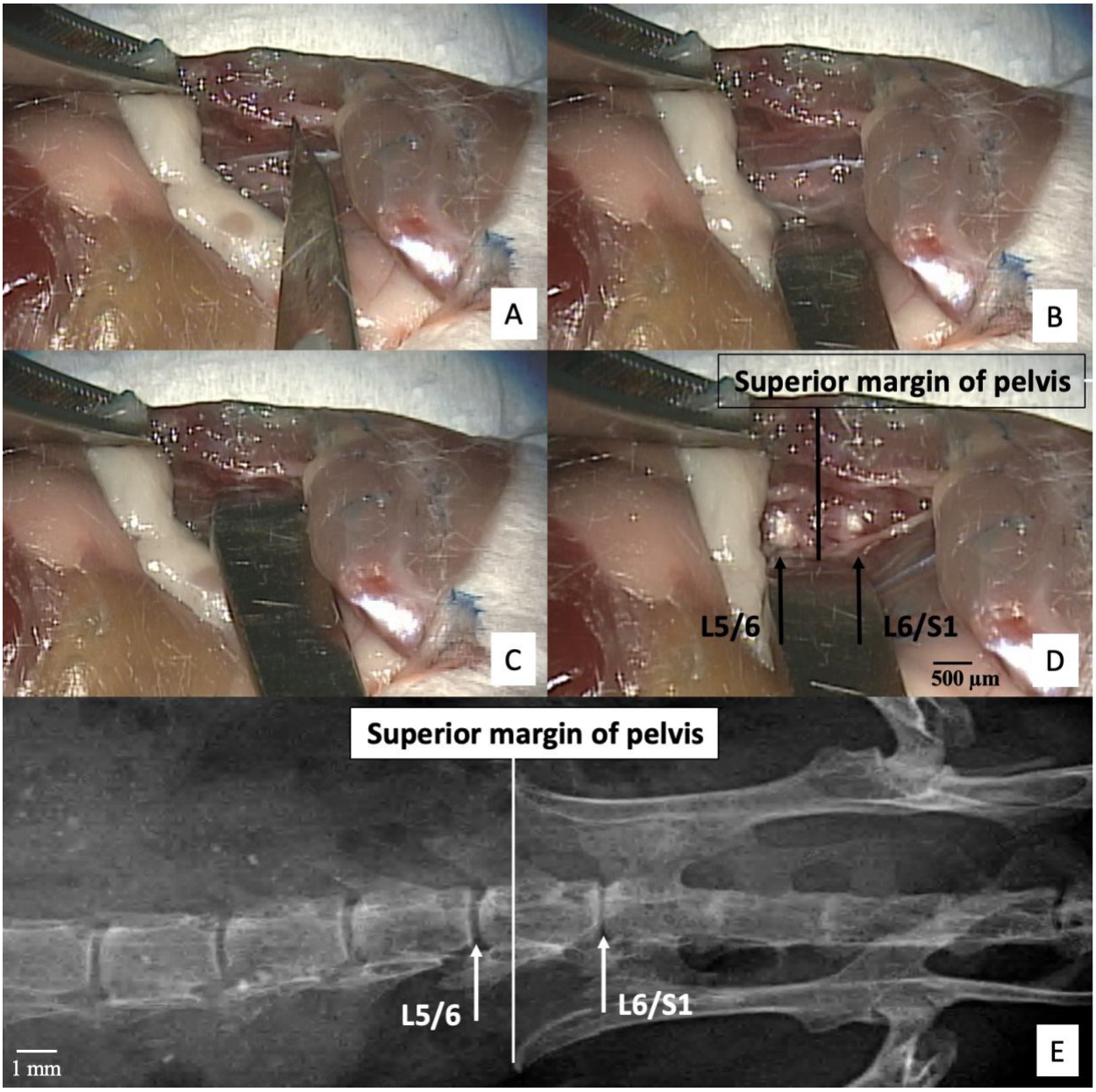

Figure 1. *Retroperitoneal dissection to expose the lumbosacral intervertebral disc using microscopic guidance*

(A) The No. 11-scalpel blade indicates the left pelvic bone and forceps grip the gluteus muscles. (**B)** The pelvis can be rotated posteriorly to increase working space by raising the gluteus muscles and rotating the left pelvic bone. The abdominal wall and peritoneum are retracted anteriorly by a Penfield dissector to

expose the psoas muscles. (**C)** The psoas muscle can be stripped posteriorly-to-anteriorly by scraping out muscles attached to the anterior surface of the pelvis with a Penfield dissector. (**D)** Superior margin of the pelvic bone indicating the L6 vertebral body. (**E**) X-ray confirms the position of the pelvis relative to the L5/6 and L6/S1 intervertebral discs.

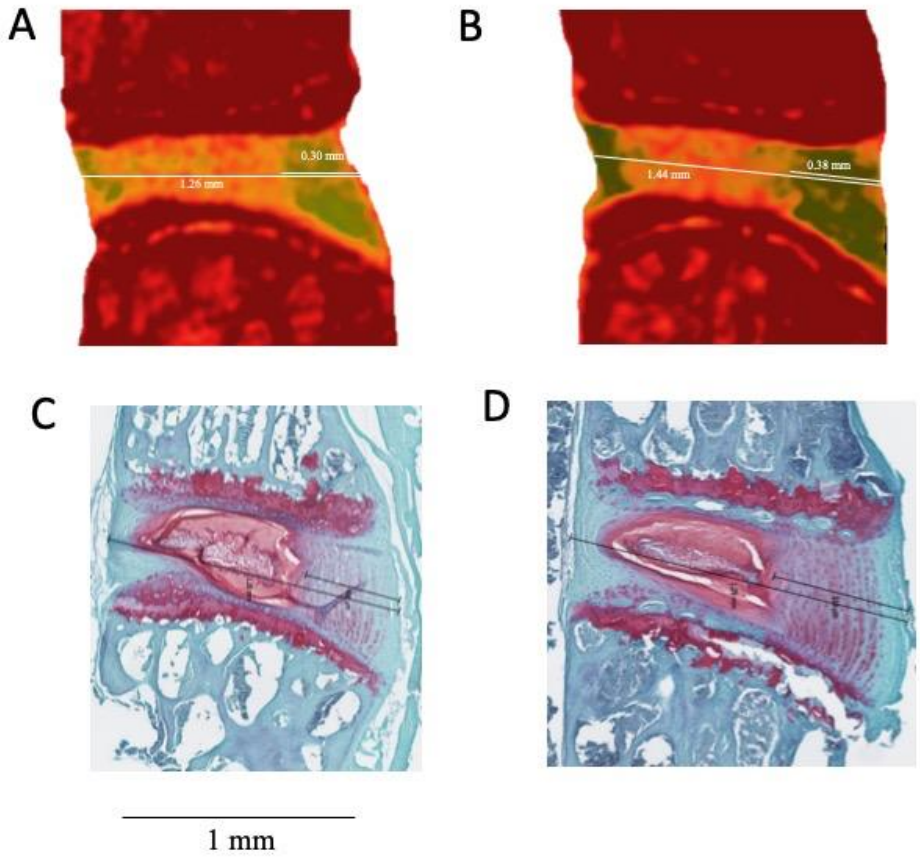

Figure 2. *Measuring the thickness of total intervertebral disc and the annulus fibrosus*

(A-B) Contrast-enhanced microCT (CEμCT) and **(C-D)** histology were used to measure the IVD widths and anterior AF thicknesses. The CEμCT and histology measurements were highly correlated ($r^2 = 0.96$, $p < 0.001$) and statistically indistinguishable (paired t-test, $p = 0.37$), confirming the fidelity of the non-destructive evaluation of CEμCT.

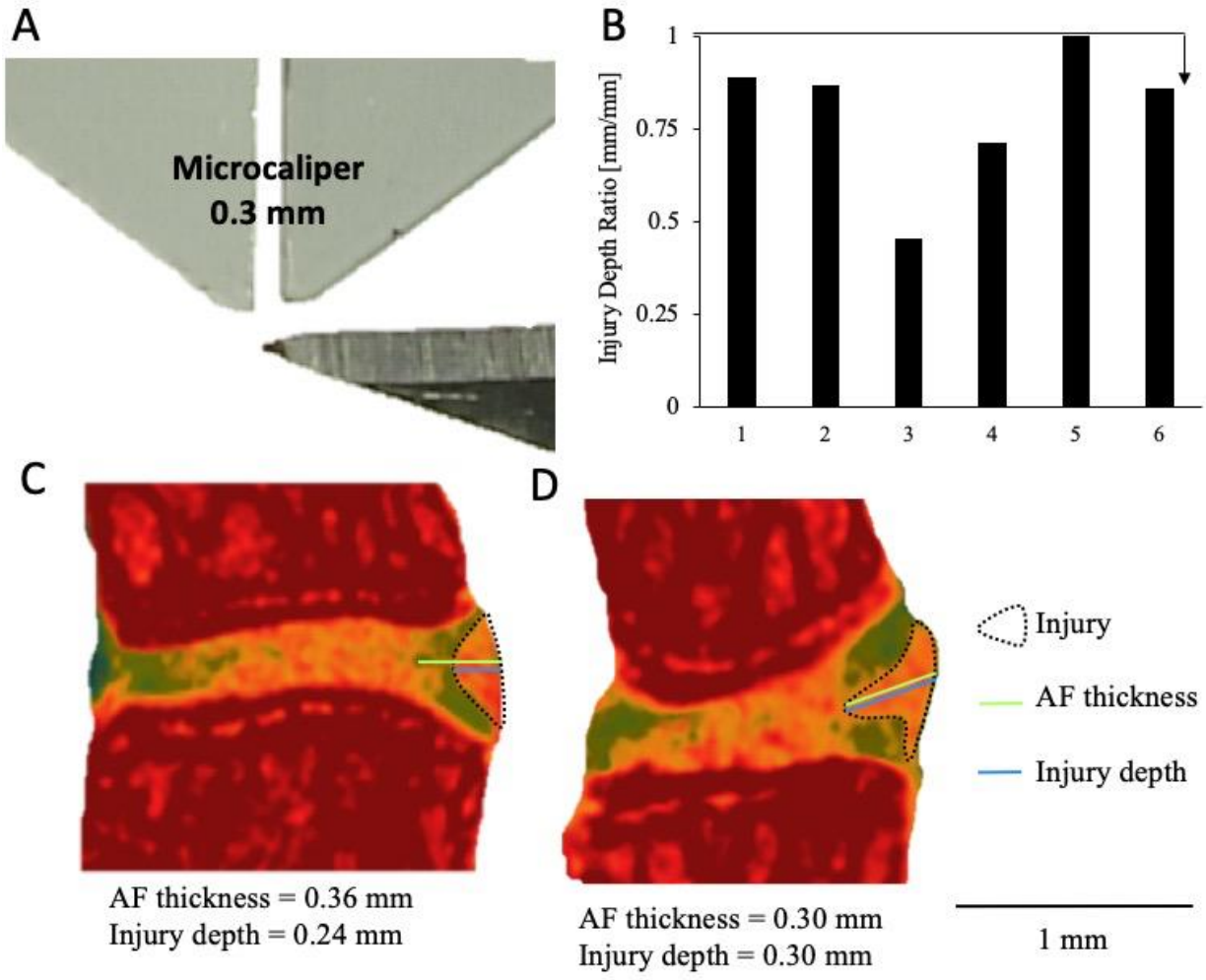

Figure 3. *Depth of the partial-width injury measured by contrast-enhanced micro-computed tomography* **(A)** The tip of the scalpel edge is marked at 0.3 mm to allow for visual confirmation during surgery that the partial-width injury is limited to the AF. **(B)** All of the injury depths were confirmed by CEμCT and histology to have depths that do not exceed of the AF in each injured IVD, confirmed by the ratio of injury depth to AF thickness which are less than 1 in all samples. **(C, D)** Representative CEμCT showing the range of depths achieved by this AF injury.

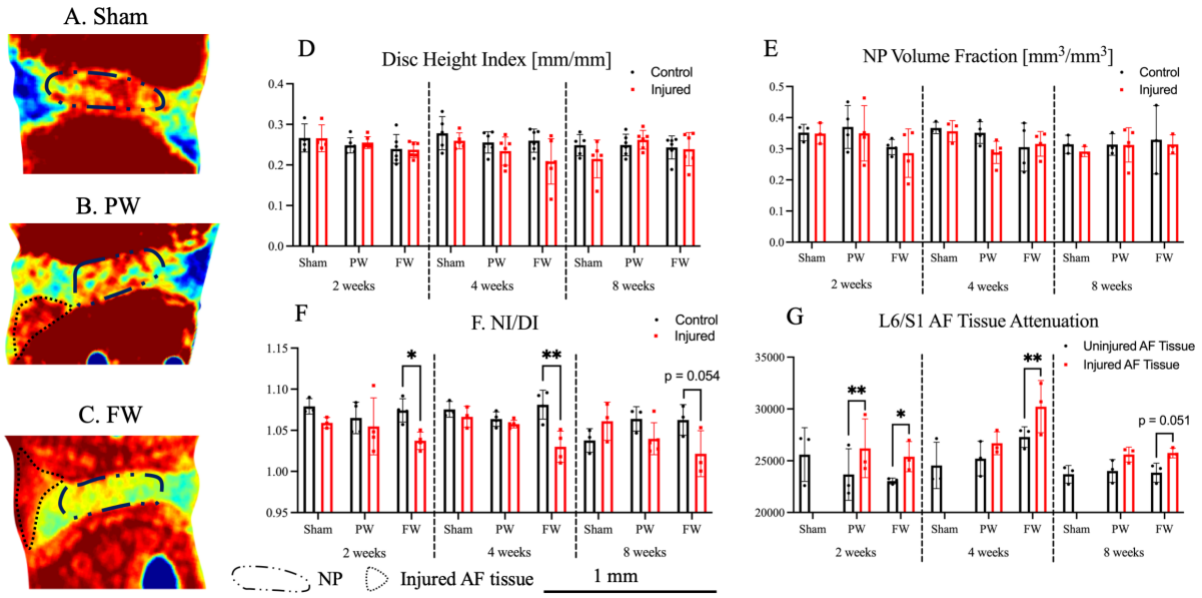

Figure 4. *Full-width (FW) injury induces a sustained loss of NP hydration compared to both the partial-width (PW) injury and Sham groups.*

(A-C) Contrast-enhanced microCT of injured level (L6/S1) where injury site is visible in both FW and PW groups. **(D)** Mean attenuation of the AF in the injured and uninjured groups. Paired t-test indicates significant increase in attenuation at injury site compared to rest of uninjured AF ($p < 10^{-5}$). **(E)** NI/DI of injured level (L6/S1) and uninjured control level (L5/6). While no changes in the whole IVD structure were detected between injured and uninjured levels with either FW or PW, the ratio of the nucleus pulposus intensity to the whole disc intensity (NI/DI – approximately 4% drop in intensity) revealed the loss hydration and proteoglycans in the nucleus pulposus of FW samples that is indicative of degeneration compared to the control IVDs.

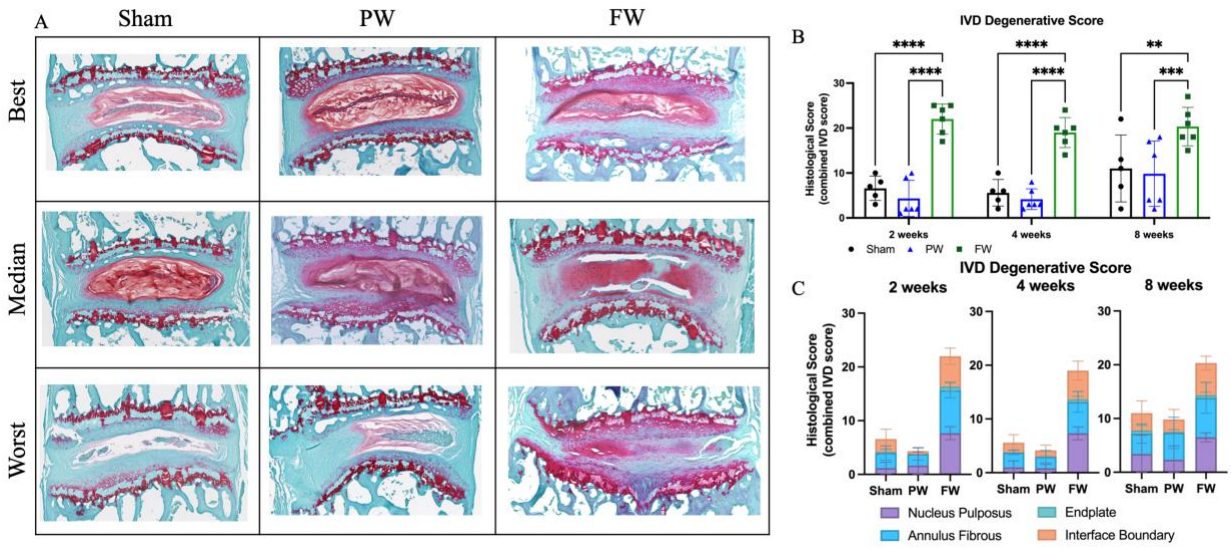

Figure 5. *FW induces quick and sustained IVD degeneration compared to both Sham and PW.* **(A)** Safranin-O stained histological section of injured level (L6/S1) **(B)** Total IVD degenerative score of L6/S1. **(C)** Breakdown of NP, AF, endplate and interface boundary contributions to total IVD degenerative score. We were unable to visualize the injury on the histological sections after the 2-, 4- and 8- week recovery timepoints. Significant degeneration was observed at all timepoints indicated by significant increases in NP, AF, interface boundary and total IVD degenerative scores in the FW group compared to Sham and PW ($p < 0.05$). While PW causes localized disruption to the AF, it does not appear to cause degeneration by eight weeks post injury.